Geochemistry Geophysics Geosystems G3
AN ELECTRONIC JOURNAL OF THE EARTH SCIENCES
Published by AGU and the Geochemical Society

Article
Volume 7, Number 11
29 November 2006
Q11022, doi:10.1029/2006GC001324
ISSN: 1525-2027

Hydrothermal exploration of the Fonualei Rift and Spreading Center and the Northeast Lau Spreading Center

C. R. German
Woods Hole Oceanographic Institution, Woods Hole, Massachusetts 02543, USA (cgerman@whoi.edu)

E. T. Baker
NOAA-PMEL, Seattle, Washington 98115, USA

D. P. Connelly
National Oceanography Centre, Southampton SO14 3ZH, UK

J. E. Lupton
NOAA-PMEL, Newport, Oregon 97365, USA

J. Resing
University of Washington, JISAO-NOAA-PMEL, Seattle, Washington 98115, USA

R. D. Prien
Institut für Ostseeforschung Warnemünde, D-18119 Rostock, Germany

S. L. Walker
NOAA-PMEL, Seattle, Washington 98115, USA

H. N. Edmonds
Marine Science Institute, University of Texas at Austin, Port Aransas, Texas 78373, USA

C. H. Langmuir
Department of Earth and Planetary Sciences, Harvard University, Cambridge, Massachusetts 02138, USA

[1] We report evidence for active hydrothermal venting along two back-arc spreading centers of the NE Lau Basin: the Fonualei Rift and Spreading Center (FRSC) and the Northeast Lau Spreading Center (NELSC). The ridge segments investigated here are of particular interest as the potential source of a mid-water hydrothermal plume (1500–2000 m depth) which extends more than 2000 km across the SW Pacific Ocean dispersing away from an apparent origin close to the most northeastern limits of the Lau Basin. Our results indicate the presence of at least four new hydrothermal plume sources, three along the FRSC and one on the NELSC, the latter situated within 150 km of the maximum for the previously identified SW Pacific regional-scale plume. However, TDFe and TDMn concentrations in the southernmost FRSC plume that we have identified only reach values of 19 and 13 nmol/L and dissolved ^{3}He anomalies in the same plume are also small, both in relation to the SW Pacific plume and to local background, which shows evidence for extensive ^{3}He enrichment throughout the entire Lau Basin water column. Our results reveal no evidence for a single major point hydrothermal source anywhere in the NE Lau Basin. Instead, we conclude that the regional-scale SW Pacific hydrothermal plume most probably results from the cumulative hydrothermal output of the entire topographically restricted Lau Basin, discharging via its NE-most corner.

Components: 7764 words, 9 figures, 3 tables.

Keywords: hydrothermal; exploration; Lau Basin; SW Pacific.

Index Terms: 3017 Marine Geology and Geophysics: Hydrothermal systems (0450, 1034, 3616, 4832, 8135, 8424); 1050 Geochemistry: Marine geochemistry (4835, 4845, 4850); 4832 Oceanography: Biological and Chemical: Hydrothermal systems (0450, 1034, 3017, 3616, 8135, 8424).

Received 4 April 2006; **Revised** 28 August 2006; **Accepted** 18 September 2006; **Published** 29 November 2006.

German, C. R., E. T. Baker, D. P. Connelly, J. E. Lupton, J. Resing, R. D. Prien, S. L. Walker, H. N. Edmonds, and C. H. Langmuir (2006), Hydrothermal exploration of the Fonualei Rift and Spreading Center and the Northeast Lau Spreading Center, *Geochem. Geophys. Geosyst.*, *7*, Q11022, doi:10.1029/2006GC001324.

1. Introduction

[2] Nearly thirty years after the first discovery of submarine hydrothermal activity [*Corliss et al.*, 1978] no more than ~10% of the ~65,000 km of global ridge crest has undergone systematic exploration for the presence and location of high-temperature venting [*Baker and German*, 2004]. Of this total, back-arc spreading centers comprise approximately 7,000 km [*Bird*, 2003] and are attracting increasing interest because here, alone, can one investigate how hydrothermal fluid compositions vary with other key variables (notably substrate and volatile composition) that cannot readily be investigated along mid-ocean ridge spreading centers [e.g., *German and Von Damm*, 2004]. The Lau Basin, in particular, is of interest in this regard because it is arguably the world's most well-constrained back-arc spreading center both in terms of its tectonophysics [e.g., *Zellmer and Taylor*, 2001] and in terms of linked geochemical and geophysical investigations [e.g., *Turner and Hawkesworth*, 1998]. It is also of special interest to vent-biologists because hydrothermal communities examined to date from the southern Lau Basin, while distinct from East Pacific Rise communities [e.g., *Desbruyeres et al.*, 1994] also share important similarities with vent-ecosystems recently located in the central Indian Ocean [*Van Dover et al.*, 2001]. Consequently, hydrothermal exploration of the SW Pacific Ocean remains a high priority for current vent biogeographic research [*Van Dover et al.*, 2002; *Tyler et al.*, 2002].

[3] The first hydrothermal vents to be located in the Lau Basin (Figure 1) were on the Valu Fa Ridge [*Fouquet et al.*, 1991] and in recent work, systematic hydrothermal exploration has been extended to cover the full length of the Valu Fa Ridge (VFR) and the East Lau Spreading Center (ELSC) [*Baker et al.*, 2005, 2006; *Martinez et al.*, 2006; *Ishibashi et al.*, 2006]. That work has revealed evidence for extensive hydrothermal activity along these southernmost sections of the Lau Basin back-arc system. In more detail, *Baker et al.* [2005, 2006] have shown that the extent of hydrothermal activity along axis also increases progressively from south to north among these segments, with increasing spreading rate, similar to that observed along mid-ocean ridge spreading centers [*Baker and German*, 2004]. In parallel work, *Baker et al.* [2005] have examined near-arc sections of three back-arc spreading centers (Valu Fa, Marianas, East Scotia Ridge) to show that, by analogy with hot-spot influenced mid-ocean ridges, certain sections of a back-arc spreading center can also exhibit anomalously low hydrothermal plume incidence, potentially related to variations in melt supply in the tectonically complex and highly variable settings of arc/back-arc intersection [see, e.g., *Livermore*, 2003; *Martinez and Taylor*, 2003].

[4] In this study we report results from a systematic investigation of two sections of back-arc spreading center from the NE Lau Basin (Figure 1): the Fonualei Rift and Spreading Center (FRSC) and the Northeast Lau Spreading Center (NELSC). The FRSC, first mapped in detail in 1996, comprises a series of rifts that are propagating south away from the Mangatolou Triple Junction (MTJ) and represent the plate boundary between the Tonga Plate and the newly recognized Niuafo'ou microplate [*Zellmer and Taylor*, 2001]. From a combination of seismic and magnetic data the FRSC has been calculated to spread at 47 mm/yr at its southernmost extent, increasing to 85 mm/yr at its northernmost limit [*Zellmer and Taylor*, 2001]. This change in spreading rate along-strike is accompanied by a systematically varying separation of the back-arc spreading center from the

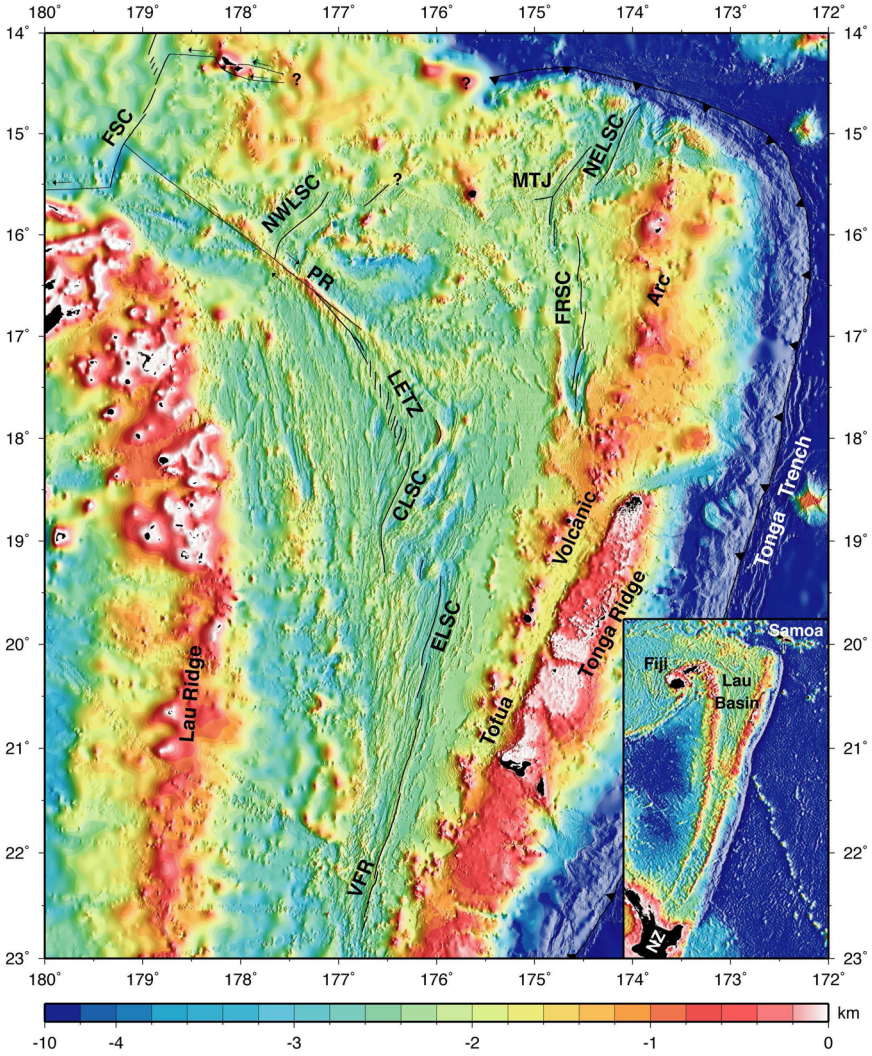

Figure 1. Regional-scale bathymetric map of the Lau Basin, SW Pacific [after *Zellmer and Taylor*, 2001] showing principal back-arc spreading centers and related tectonic features. VFR, Valu Fa Ridge; ELSC, East Lau Spreading Center; CLSC, Central Lau Spreading Center; LETZ, Lau Extensional Transform Zone; PR, Peggy Ridge; FSC, Futuna Spreading Center; NWLSC, Northwest Lau Spreading Center; FRSC, Fonualei Rift and Spreading Center; MTJ, Mangatolou Triple Junction; NELSC, Northeast Lau Spreading Center. The NE Lau Basin, specifically, the FRSC and NELSC, forms the focus for this investigation.

adjacent Tonga arc, ranging from ~25 km at 18°S to ~75 km at 16°S, approximately 220 km farther north. This is directly analogous to the variations seen along the VFR and ELSC where separations between arc and back-arc vary from 40 to 120 km as back-arc spreading rates increase from 40 to 90 mm/yr. One particular difference between the VFR/ELSC and the FRSC, however, is that along the VFR/ELSC the observed variations progress more gradually along almost double the length of ridge axis between 23°S and 19°S (Figure 1).

[5] The Northeast Lau Spreading Center (NELSC) lies north of the MTJ extending toward the northernmost Tonga Trench (Figure 1). This segment represents one of three major spreading centers in the northernmost Lau Basin, along with the Futuna Spreading Center (FSC) and the Northwest Lau Spreading Center (NWLSC). Although the recent three-plate kinematic model of the Lau Basin [*Zellmer and Taylor*, 2001] does not encompass this region north of 15.5°S, it is clear from existing data that additional microplates and/or deformation zones must be present [*Pelletier et al.*, 2001]. What is known (from GPS studies) is that the total separation rate between the Australia and Tonga plates at this latitude, orthogonal to the strike of the NELSC, is 157 mm/yr and that of this total, spreading at the MTJ (from magnetics) is 94 mm/yr,

similar to the northern FRSC [*Zellmer and Taylor*, 2001]. Because the NE branch of the MTJ connects via a large overlapper with the parallel-striking NELSC, we assume that maximum spreading rates along the NELSC are also ~94 mm/yr but that, as with other overlapping spreading centers, spreading rate decreases to zero at the tips of each limb. In addition to extending the full length of back-arc spreading center surveyed, there are two further reasons for our particular interest in investigating the NELSC for hydrothermal activity. First, there is the possibility that the northernmost NELSC might be affected by the nearby Samoan hot-spot and that this might affect local melt supply in such a way as to cause anomalies in detectable hydrothermal plume incidence. Similar processes have been invoked previously to explain the low incidences of hydrothermal plume signals reported from along arc-adjacent sections of the fast-spreading East Scotia Rise [*German et al.*, 2000; *Baker et al.*, 2005].

[6] Perhaps of greatest significance, however, is that the NELSC is a potential source for one of the three most significant ^{3}He-enriched hydrothermal plumes throughout the entire Pacific Ocean. *Lupton et al.* [2004] have recently identified this SW Pacific plume, which is centered at ~1500–1800 m and extends northwest for more than 2000 km away from a source located between the Samoa Islands and the northern Lau-Havre Trough. Specifically, the strongest single profile of dissolved ^{3}He/^{4}He anomaly analyzed in that work was located at 15.0°S, 173.1°W with maximum signal strength at 1726 m depth (Figure 2). Stations farther west along this 15°S transect, including one station occupied directly above the FSC (Figure 1) showed progressively decreasing concentrations, while those east of the Tonga arc showed no evidence of a ^{3}He-rich plume at these water depths. Because the observed plume maxima were observed at 1480–1790 m water depth, *Lupton et al.* [2004] concluded that the likely source for this material should be located at a depth of 1450–1950 m. This is both too shallow to implicate hydrothermal plumes sourced along a typical mid-ocean ridge (southern EPR plume [cf. *Lupton and Craig*, 1981]) but also up to 1000 m too deep to be the result of any local arc-related hydrothermal plumes such as those recently reported to be emanating from close to the summit of Vailulu'u Seamount [*Hart et al.*, 2000; *Staudigel et al.*, 2006], believed to be the current locus of the Samoa hot-spot. Consequently, *Lupton et al.* [2004] concluded that the source for this major ^{3}He-rich plume was most probably associated with the back-arc spreading center systems of the NE Lau Basin and, more specifically, with the ridge-sections closest to the Mangatolou Triple Junction where spreading rates are high (~94 mm/yr) and the depth of the ridge-crest spans the relevant plume-depths, from 1500–1900 m.

2. Methods

[7] All sampling was conducted during the final phase of cruise KM0417 of the R/V *Kilo Moana*, October 2004 [*Langmuir et al.*, 2005]. The principal method of hydrothermal investigation was to use Miniature Autonomous Plume Recorders (MAPRs) mounted on a series of rock-core (RC ###) and/or dredge (DR ##) stations occupied along the length of the Fonualei Rift and Spreading Center (FRSC) and the Northeast Lau Spreading Center (NELSC), as targeted from multi-beam bathymetry (Figure 2). The location of each MAPR station is listed in Table 1 along with sampling time (Julian Day, 2004 and time of arrival at the seafloor) and water depth. For dredge stations, the locations and times for the dredge leaving the seafloor are also reported.

[8] MAPRs have been widely used on rock core and dredge operations to detect hydrothermal plumes [e.g., *Scheirer et al.*, 1998; *Baker et al.*, 2001a; *Edmonds et al.*, 2003]. MAPRs record both in situ temperature and light backscattering, but normally cannot resolve the very small temperature anomalies characteristic of weak, nonbuoyant hydrothermal plumes (calculation of hydrothermal temperature anomalies requires conductivity as well as temperature). The light backscattering circuit is calibrated alone by applying a known voltage at several points over the full-scale range 0.0–5.0 V, and the output is fit to a least squares linear regression (r^2 typically > 0.99). Light backscattering measurements are relative rather than absolute measures of the light backscattering coefficient and can differ slightly among individual sensors [*Baker et al.*, 2001b]. A factor unique to each sensor (a_n) is determined separately from a laboratory calibration using formazine [*Baker et al.*, 2001b]. MAPR data, converted to volts, are reported in terms of nephelometric turbidity units (NTUs) [*American Public Health Association*, 1985] according to the expression

$$\Delta\mathrm{NTU} = (V_r - V_b)/a_n,$$

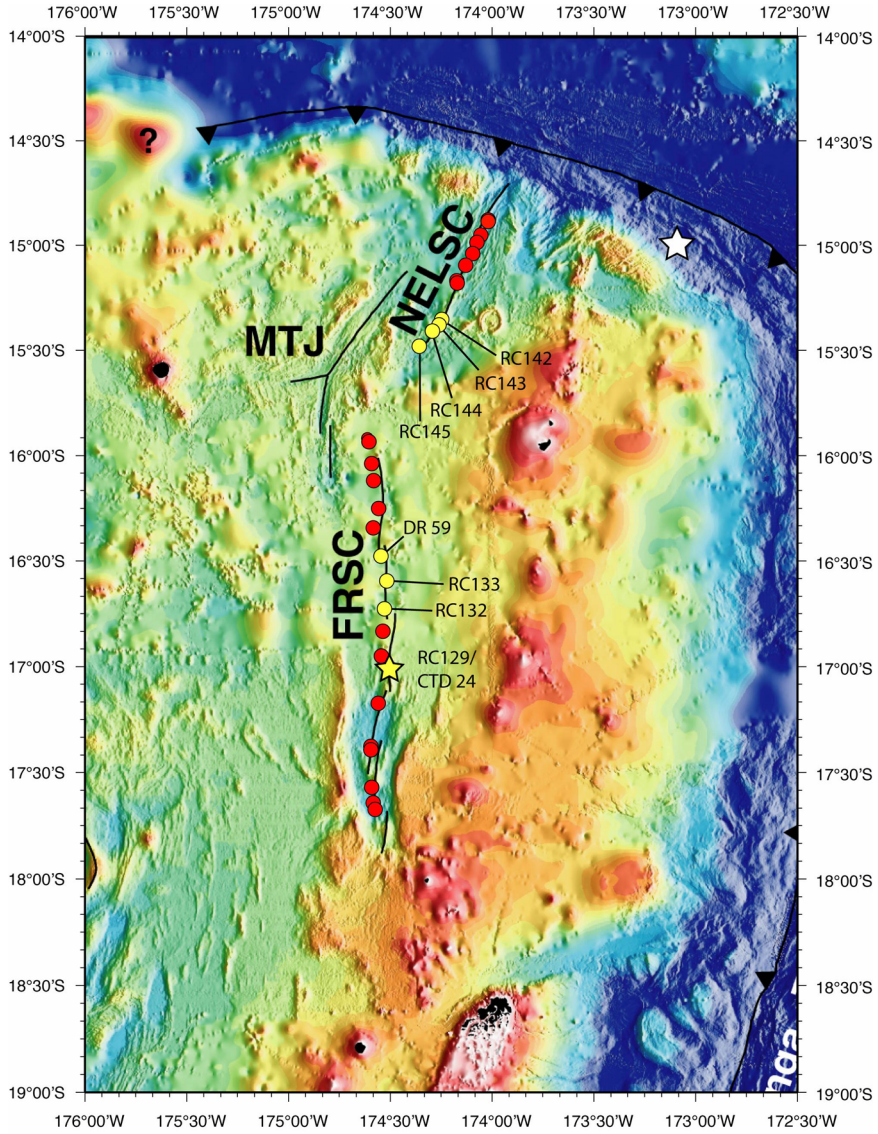

Figure 2. Detailed map of the NE Lau Basin showing locations (circles) of MAPR stations. Yellow and red symbols indicate, respectively, stations with and without optical backscatter (ΔNTU) anomalies indicating the presence of nonbuoyant hydrothermal plumes (for dredge stations, adjacent/overlapping symbols represent locations of upcast and downcast). Also shown are the location of CTD 24 (yellow star) occupied on the FRSC during this study (obscuring the yellow circle for station RC 129) and the CTD station at 15.0°S, 173.1°W (white star) from which highest δ^3He anomalies measured anywhere in the regional-scale SW Pacific hydrothermal plume were reported [*Lupton et al.*, 2004]. Bathymetry: see Figure 1 for scale.

where ΔNTU is the plume light backscattering anomaly above ambient, V_r is the raw voltage reading of the sensor, and V_b is the background voltage of ambient water not affected by hydrothermal plumes. Field calibrations with these sensors have shown that for typical deep-sea particles the mass concentration $C_m = -0.003 + 0.39(\Delta NTU)$, $r^2 = 0.97$ [*Baker et al.*, 2001b]. The same sensor type was also used on CTD cast 24, independent of the MAPRs.

[9] Analysis of MAPR profiles from stations where no plumes were encountered found that a 1σ variability of the ΔNTU signal was typically = 0.0013 over the depth range of 800–1700 m, where plumes were found. We use a detection limit of 3σ to confidently identify a ΔNTU hydrothermal signal, thus requiring a ΔNTU $\geq$ 0.004 above background at any station. Note that the background NTU varies slightly both vertically and regionally, an inherent consequence of the

Table 1. MAPR Sampling Stations[a]

Station	Day	Time	Latitude, S	Longitude, W	Depth, m
FRSC					
DR 57	286	0831	17°49.33′	174°31.90′	1871
		0925	17°49.30′	174°31.99′	
RC 125	286	1400	17°39.39′	174°34.60′	2865
RC 126	286	1521	17°41.27′	174°33.93′	2552
RC 127	286	1716	17°35.00′	174°35.00′	2122
DR 58	286	2058	17°23.38′	174°35.28′	2743
		2157	17°24.34′	174°35.19′	
RC 128	287	0053	17°11.20′	174°33.01′	2113
RC 129	287	0300	17°01.50′	174°30.12′	1667
RC 130	287	0415	16°57.81′	174°32.19′	1496
RC 131	287	1156	16°50.79′	174°31.74′	1730
RC 132	287	1320	16°44.49′	174°31.20′	1713
RC 133	287	1514	16°36.49′	174°30.56′	1980
DR 59	287	1823	16°29.49′	174°32.71′	2419
		1945	16°29.52′	174°32.32′	
RC 134	287	2148	16°21.48′	174°34.52′	1878
RC 135	287	2330	16°15.97′	174°33.00′	2056
RC 136	288	0128	16°08.01′	174°34.47′	2045
RC 137	288	0250	16°03.19′	174°35.00′	2463
DR 60	288	0540	15°55.99′	174°36.21′	2066
		0647	15°56.44′	174°35.82′	
NELSC					
DR 61	288	1539	14°53.51′	174°00.71′	2921
		1628	14°54.02′	174°00.71′	
RC 138	288	1829	14°57.84′	174°02.80′	2565
RC 139	288	2020	15°00.04′	174°04.01′	2829
RC 140	288	2302	15°03.20′	174°05.24′	2672
RC 141	289	0040	15°06.47′	174°07.33′	2330
DR 62	289	0217	15°10.98′	174°09.87′	2049
		0315	15°11.58′	174°09.79′	
RC 142	289	0628	15°22.04′	174°14.41′	1491
RC 143	289	0735	15°23.55′	174°15.20′	1665
RC 144	289	0833	15°25.32′	174°17.12′	1626
RC 145	289	1003	15°29.62′	174°20.99′	2165

[a] DR, dredge; RC, rock core.

distribution of fine-grained particles in the water column.

[10] At each station, a MAPR on the dredge or rock core wire was lowered to within 50 m or less of the seafloor to obtain vertical profiles of NTU. In total, 26 sets of MAPR deployment were completed (Table 1, Figure 2). First, a series of 16 stations (2 dredges and 14 rock-cores) were occupied along ~185 km of the FRSC that strikes almost due north-south, extending from ~15°50′S to nearly 18°00′S along ~174°30′W. This yielded an average spacing of one MAPR profile every ~13 km (±5 km, 1σ) with gaps in excess of 20 km between adjacent stations on just two occasions (21 km and 24 km). Next, a further 10 stations were occupied along the ~75 km of NE-SW trending NELSC between 14°53.5′S 174°0.7′W and 15°29.6′S 174°21.0′W. The average spacing between these stations was ~7.5 km (±5 km, 1σ) with only one gap greater than 10 km (20.6 km).

[11] Although we were primarily reliant upon optical backscatter signals from MAPRs to detect hydrothermal plumes in this study, a CTD-station (CTD 24) was also occupied at the first site on the FRSC that yielded significant optical backscatter signals (Figure 2). The CTD used was a SeaBird 911+ equipped with a SeaPoint optical backscatter sensor together with a 24-position rosette, from which a 13 point profile of water-column samples was collected using 10-litre acid-cleaned Niskin bottles. These samples were subsequently analyzed for dissolved ^{4}He concentrations and ^{3}He/^{4}He ratios in the Helium Isotope Laboratory, NOAA PMEL, Newport, Oregon [*Lupton*, 1990] and for total dissolvable Fe and Mn concentrations (TDFe and TDMn) [*Magnusson and Westerlund*, 1981] at the National Oceanography Centre, Southampton

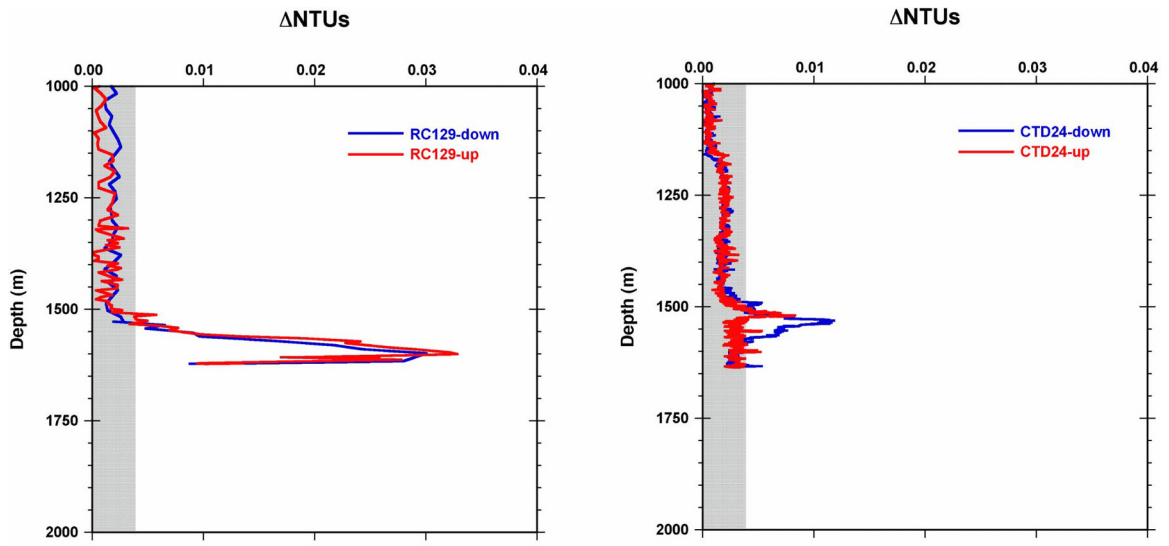

Figure 3. Deep-water (>1000 m) profiles of optical backscatter (ΔNTU) measured above the southern FRSC near 17°01.5′S during (left) RC129 and (right) subsequently occupied CTD 24. Station locations are listed in Table 1 and shown in Figure 2. Gray shading indicates background optical backscatter values (ΔNTU < 0.004).

(UK). Samples taken for He analysis were drawn into copper tubing on board ship using a special hydraulic crimping device [*Young and Lupton*, 1983]. Due to shortage of sampling bottles at this late stage of the cruise, not all 13 bottles sampled for He isotopes were also sampled for TDMn and TDFe. Instead, because nonhydrothermal background levels had already been well-established for the SW Pacific Ocean, two of the four above-plume samples were omitted from the TDMn and TDFe sampling. In addition to the water samples described above, four further samples were taken for suspended particulate analyses. These samples, targeted from in-situ NTU signals, were taken from duplicate Niskin bottles tripped at each of four depths within the optically defined plume. All particulate matter was collected onto 0.4 μm acid-washed poly-carbonate Nucleopore filters by pressure filtration. Samples (4–8 L seawater) were transferred to acid-cleaned pressure filtration reservoirs which were pressurized using purified air. Filters were rinsed with de-ionized water, buffered to pH 8 with quartz distilled NH_4OH, to remove seawater salts. Elemental composition of particulate matter was determined by x-ray primary- and secondary-emission spectrometry with a Pd source and Mo, Ti, Ge, and Co secondary targets using a nondestructive thin-film technique [*Feely et al.*, 1991].

[12] On the NELSC one further CTD station was attempted following detection of an even stronger optical backscatter anomaly at station RC 143 (Figure 2). This station had to be abandoned, however, due to deteriorating weather conditions; two final rock-core stations (RC 144 and RC 145) were occupied instead [*Langmuir et al.*, 2005].

3. Results and Discussion

3.1. Optical Backscatter Anomalies

[13] Along the FRSC only four out of sixteen MAPR stations (RC 129, 132, 133 and DR59) revealed significant (≥0.004 ΔNTU) optical backscatter signals indicative of nonbuoyant hydrothermal plumes (Figures 2, 3, and 4). On the NELSC, four of ten stations (RC 142–145) also revealed significant plume-signals (Figures 2 and 5). Although eight "positive" plume-profiles were obtained throughout our study, however, they likely represent evidence for no more than four discrete hydrothermal sources, three along the FRSC and one more on the NELSC. The most southerly source was detected on RC 129 and CTD 24. Both these stations were occupied at essentially the same location (17°01.5′S, 174°30.1′W) with the ship operating in dynamic positioning mode. Despite this dual occupation, only a few hours apart, the plume intensity and vertical distribution changed markedly between RC 129 and CTD 24, and even during CTD 24 (Figure 3). Maximum ΔNTU values exceeded 0.030 on RC 129, but were both <0.020 and 50–75 m shallower on CTD 24. Such temporal variability is not uncommon when profiling a plume very close to its source, because even

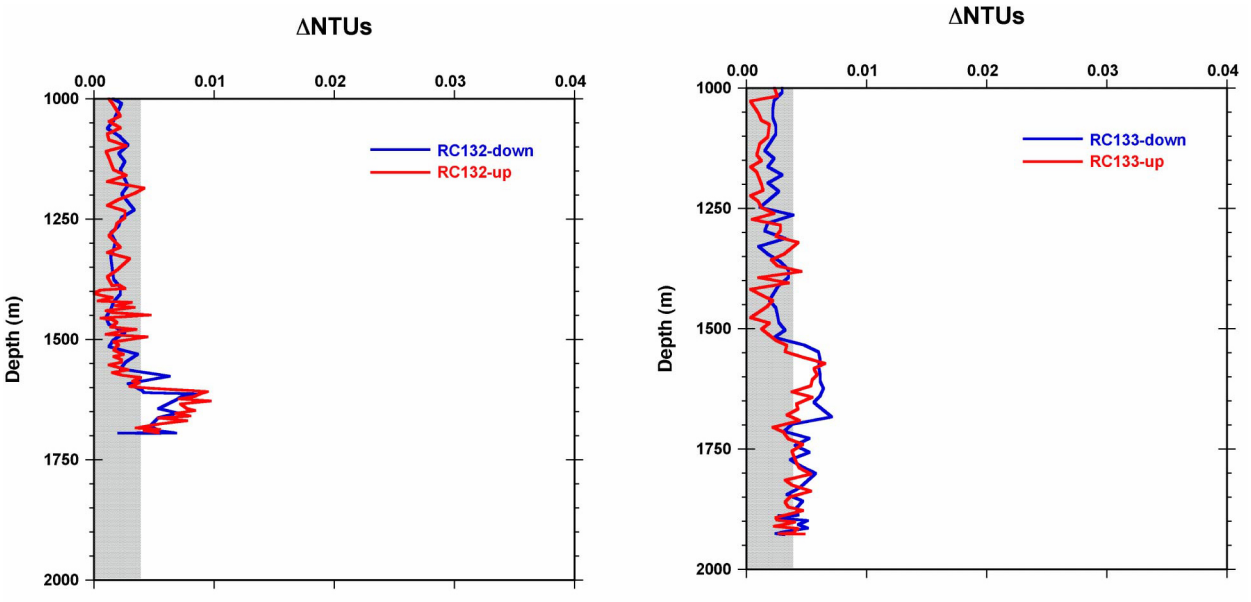

Figure 4. Deep-water (>1000 m) profiles of optical backscatter (ΔNTU) measured above the central FRSC between 16°45′S and 16°36′S at stations (left) RC 132 and (right) RC 133. Station locations are listed in Table 1 and shown in Figure 2. Note that maximum plume anomalies for RC 132 are greater than those for RC 133 and occur over a more restricted, less diffuse depth range. Gray shading indicates background optical backscatter values (ΔNTU < 0.004).

small changes in current speed and direction can substantially alter the height and flow of a nonbuoyant plume. For example, differences in depth between the plumes observed during RC 129 and CTD 24 are less than 100 m and can be reconciled readily by tidal variations in the height of a single nonbuoyant hydrothermal plume over the 5–7 hour interval that elapsed between occupation of the two stations, or even within the 2 hour duration of CTD 24 [cf. *Rudnicki et al.*, 1994; *Rudnicki and German*, 2002; *Walker et al.*, 2004]. Close to the source, particle concentrations might also change within the nonbuoyant plume because the oxidation kinetics for precipitation of freshly emitted dissolved Fe(II) should be slow compared to the timescale for plume emplacement in the SW Pacific Ocean [*Field and Sherrell*, 2000; *Statham et al.*, 2005]. In conclusion, the data reported here are consistent with a locally sourced hydrothermal plume, close to 17° 01.5′S on the FRSC, rising 75–150 m above the seabed.

[14] Evidence for a second hydrothermal source on the FRSC comes from rock core stations RC132 and 133. Both stations show a weak (<0.01 ΔNTU) plume centered between 1550 and 1700 m (Figure 4). The sharper, more intense characteristics of the plume at RC132 suggest that station may be closer to the source than RC133. A third FRSC source was identified from a cross-axis (174°32.7–32.3′W) dredge in water depths shallowing from 2420 to ~2000 m at 16°29.5′S (Figure 5). DR59 found intense plumes (maximum ΔNTU

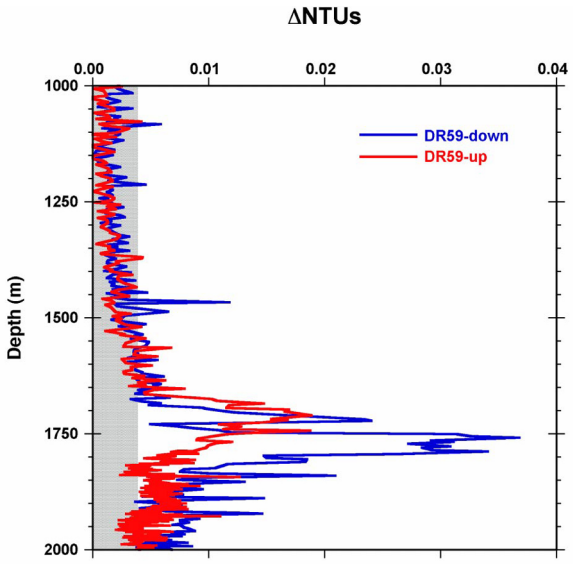

Figure 5. Deep-water (>1000 m) profiles of optical backscatter (ΔNTU) measured above the central FRSC near 16°30′S at station DR59. Downcast and upcast locations are listed in Table 1 and shown in Figure 2. Gray shading indicates background optical backscatter values (ΔNTU < 0.004).

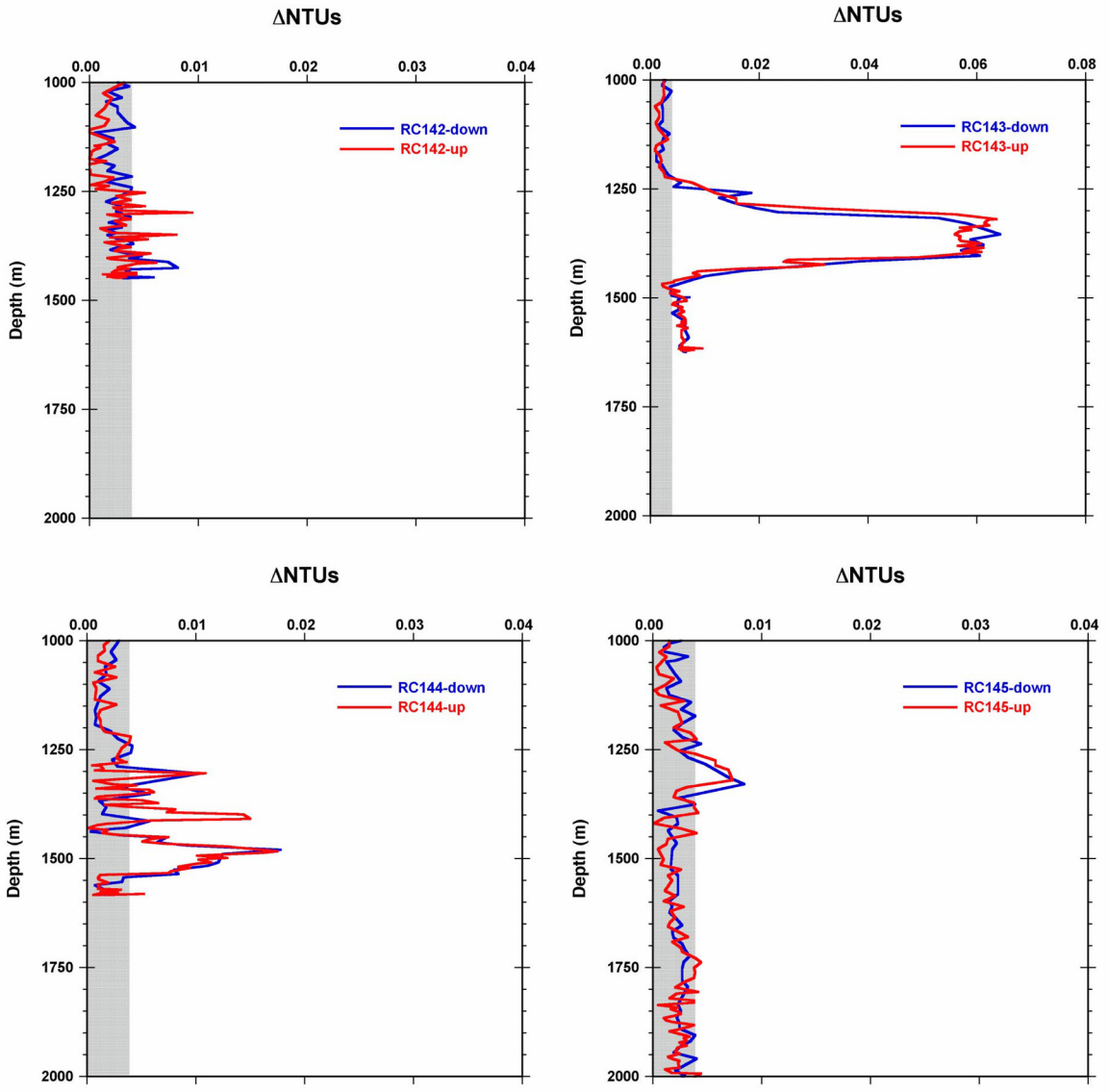

Figure 6. Deep-water (>1000 m) profiles of optical backscatter (ΔNTU) measured above the NELSC at stations (top left) RC142, (top right) RC143, (bottom left) RC 144, and (bottom right) RC 145. Note change in ΔNTU scale for RC143 when compared to all other stations presented in Figures 3–6. Station locations are listed in Table 1 and shown in Figure 2. Gray shading indicates background optical backscatter values (ΔNTU < 0.004).

~0.038) on two profiles spaced ~700 m apart, during the deployment and recovery of the dredge. As for RC129/CTD24, the down- and up-profiles for DR59 also showed substantial variability over short scales in both time and distance. While we cannot be certain that the plumes at these three adjacent stations do not all emanate from a single source, the similarities of RC132 and 133 (Figure 4), the distinctiveness of DR59 (Figure 5), and the 27 km distance separating DR 59 from RC132 along axis (Figure 2) all lead us to conclude that these plumes result from two distinct sources on the FRSC.

[15] The strongest plume-signals observed from any of our MAPR deployments were on the NELSC at stations RC 142–145 (Figure 6). Here, maximum plume anomalies were approximately double those observed in any of the plume signals detected along the FRSC. At RC 143 (15°23.55′S, 174°15.20′W, 1665 m water depth) maximum plume values of >0.06 ΔNTU were observed at 1300–1400 m, with above-background values observed at all depths below ~1225 m. At adjacent stations RC 142, 144, and 145, much reduced plume signals were observed (ΔNTU < 0.02). These data provide excellent constraints on the

Table 2. CTD24 Water-Column Analyses

CTD Bottle	Depth, m	[He-3], cc STP/g	[He-4], cc STP/g	del (3He), %	TDFe, nmol/kg	TDMn, nmol/kg
23	497	5.59E-14	3.96E-08	1.6	0.9	1.1
22	744	5.88E-14	4.01E-08	5.5	not taken	not taken
20	991	6.76E-14	4.17E-08	16.8	0.5	1.0
19	1239	7.58E-14	4.27E-08	27.6	not taken	not taken
17	1486	8.15E-14	4.30E-08	36.2	14.6	5.3
15[a]	1504	8.23E-14	4.29E-08	38.1	17.0	10.1
13[a]	1515	8.45E-14	4.34E-08	40.1	11.7	11.3
11[a]	1521	8.47E-14	4.32E-08	40.9	18.8	13.4
9[a]	1535	8.36E-14	4.32E-08	39.4	3.1	0.9
7	1555	8.39E-14	4.31E-08	40.0	7.7	2.0
5	1564	8.43E-14	4.33E-08	40.1	14.2	5.3
3	1584	8.38E-14	4.32E-08	39.7	20.7	11.9
1	1634	8.38E-14	4.33E-08	39.3	11.7	8.8

[a] Duplicate bottles sampled for particulate analyses; see Table 3.

lateral extent of this plume over 15–20 km along-axis and indicate that venting may have been most closely approached at station RC 143. While the strength of the plume at RC143 suggests a proximal source, however, the depth at which that plume is observed suggests a source on the seafloor at just 1400–1500 m, assuming a height of rise of 100–200 m comparable to other Lau Basin hydrothermal plumes [e.g., *German et al.*, 2004; *Edmonds et al.*, 2004]. While the plume-depth data suggest a source depth much shallower than the 1665 m water depth encountered at RC143, however, the NELSC axis shallows dramatically NE of this station, reaching 1491 m depth at station RC 142, just 3 km distant. In combination, therefore, the depth and intensity of this plume suggest that the source of this, the strongest plume detected anywhere in our survey, is located within a few km of station RC143, most probably along the very shallowest section of the NELSC between stations RC143 and RC142 (15° 22.0–23.5′S, 174° 14.4–15.2′W; Table 1).

3.2. Geochemical Signals of Hydrothermal Activity

[16] To characterize the mid-water ΔNTU signals we observed and to investigate their hydrothermal nature in more detail, it was important to collect water and suspended particulate samples from at least one location where significant plume signals had been observed. This was achieved at station CTD 24: a reoccupation of the site identified from RC129 (Table 1; Figure 2). Here a 13-point profile of water samples was collected and samples analyzed for dissolved helium isotope abundances, TDFe and TDMn (Table 2). All three tracers show extremely good correlations with the ΔNTU profile from the upcast of CTD 24, during which the water samples were taken (Figure 7). For TDFe, concentrations increase to a maximum of 18.8 nmol/l at the depth of the particle maximum compared to a background concentration of ≤1.0 nmol/l. For TDMn a similar trend is observed with maximum concentrations at plume-height reaching 13.4 nmol/l compared to background concentrations of ∼1.0 nmol/l. In addition to total dissolvable Fe and Mn concentrations, which we report throughout the CTD 24 profile, four samples were also collected around the ΔNTU maximum, identified in situ during the course of the CTD cast, for filtration and analysis of suspended particulate (>0.45 μm) concentrations (Fe, Mn, S, Ca, Mg, Al and Si). Those analyses (Table 3) reveal that particulate Fe concentrations are typically ∼10 nmol/L, representing ≥50% of total Fe concentrations in the ΔNTU plume at the time of on-deck sample processing (see below). By contrast, particulate Mn concentrations are closer to 1 nmol/L and represent only ∼10% of total Mn concentrations at these depths.

[17] Below the ΔNTU plume, where no sampling was conducted for suspended particulate matter, TDFe and TDMn concentrations are also high and the dissolved ^{3}He profile correlates well with these maxima as well as the ΔNTU peak at ∼1520 m (Figure 7), confirming that both metal-rich layers are hydrothermal in origin. Why should this be? Operationally defined "total dissolvable" metal concentrations represent both the dissolved Fe and Mn in any given sample *and* their concentrations in readily dissolvable particulate fractions. For any hydrothermal plume sample with high TDFe concentrations but no accompanying NTU anomalies (indicative of suspended particulate ma-

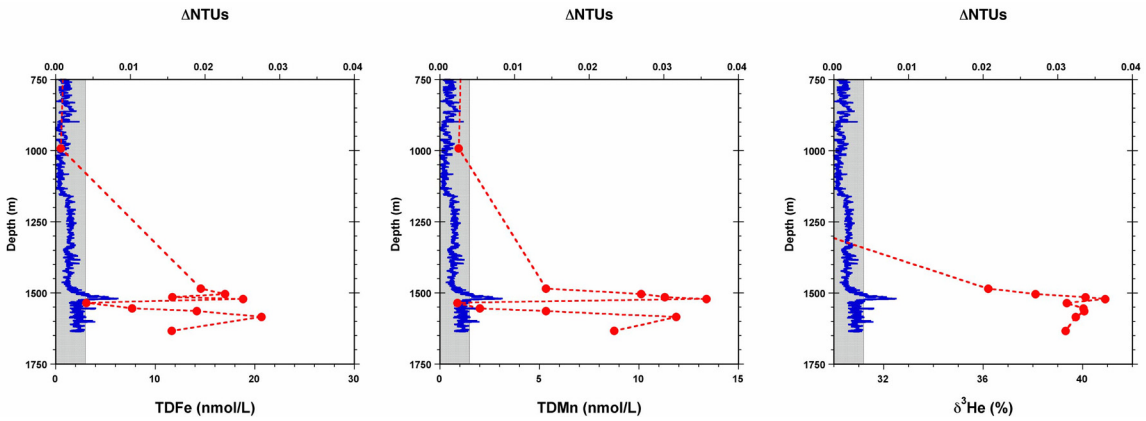

Figure 7. Deep-water (>1000 m) profiles of total dissolvable Fe, total dissolvable Mn, and δ^3He anomalies as measured in samples collected during the upcast at station CTD 24 on the FRSC. Corresponding ΔNTU values for the CTD 24 upcast are also shown for comparison: gray shading indicates background optical backscatter values (ΔNTU < 0.004).

terial), therefore, the simplest explanation is that the Fe present occurs primarily as unoxidized dissolved Fe(II) rather than as suspended particulate Fe-oxyhydroxides. The collection of significant TDFe concentrations in the deep samples of CTD24, therefore, in the absence of any co-registered ΔNTU signals, provides further evidence that this station was located close (≤1 km) to a source of active venting. As described in the previous section, oxidation of hydrothermally released dissolved Fe(II) in the SW Pacific Ocean is slow (order hours) compared to emplacement within the nonbuoyant plume [*Field and Sherrell*, 2000; *Statham et al.*, 2005]. The shallow plume samples at CTD24, targeted from ΔNTU signals, would then represent nonbuoyant plume waters that were relatively "old" (thus particle rich) when compared to the Fe- and Mn-rich, but particle poor, samples collected from deeper in the water column.

[18] Of course, just because ΔNTU signals may not reveal all components of a hydrothermal plume, this does not invalidate the MAPR-based hydrothermal exploration techniques that we have employed consistently for Mid-Ocean Ridge research over the past decade [e.g., *Scheirer et al.*, 1998; *German et al.*, 1998; *Baker et al.*, 2001a, 2006; *Edmonds et al.*, 2003]. Even for the least-oxidizing hydrothermal plume environments likely to be encountered in the modern deep-ocean we would predict that more than 50% of all dissolved Fe(II) injected into a nonbuoyant hydrothermal plume will be oxidized to form suspended particulate Fe-oxyhdyroxides within 8 hours (NE Pacific [*Field and Sherrell*, 2000]). Hence, assuming ~1 hour for buoyant plume rise and typical dispersion currents of 2–4 cm/sec, we should expect to be able to detect ΔNTU signals within a nonbuoyant hydrothermal plume before it has dispersed more than 0.5–1.0 km from its active vent-source along *any* ridge-crest. It is for this reason that ΔNTU signals can be relied upon to provide first-order information on the presence or absence of ridge-crest hydrothermal activity, throughout the world's ocean basins, to within a length scale of some kilometers. If a vent-site is particularly closely approached, however, ΔNTU signals and chemical anomalies can become decoupled.

[19] In the δ^3He profile (Figure 7), the highest value observed is ~41%, at 1520 m; δ^3He values of ~40% are also observed in the deeper, TDFe- and TDMn-rich plume. Unlike the case for TDMn and TDFe, however, these δ^3He plume enrichments are not superimposed upon constant low background values above plume height. Rather, examination of the full δ^3He profile (Figure 8) shows that the marked and well-characterized plume-anomaly clearly evident in Figure 7 is superimposed upon a much broader background gradient that increases from δ^3He = 5.5% at 744 m to 39.3%

Table 3. Particulate Metal Concentrations at CTD 24[a]

Sample Depth, m	Fe	Mn	S	Ca	Mg	Al	Si
1504	9.7	1.2	9.0	26.0	5.5	11.1	30.3
1515	10.5	1.4	10.7	25.8	5.2	12.2	32.8
1521	9.1	1.1	11.8	21.9	5.6	10.7	25.9
1535	8.9	1.6	8.0	21.9	4.2	10.5	22.5

[a] Units for all elements are nmol/L seawater.

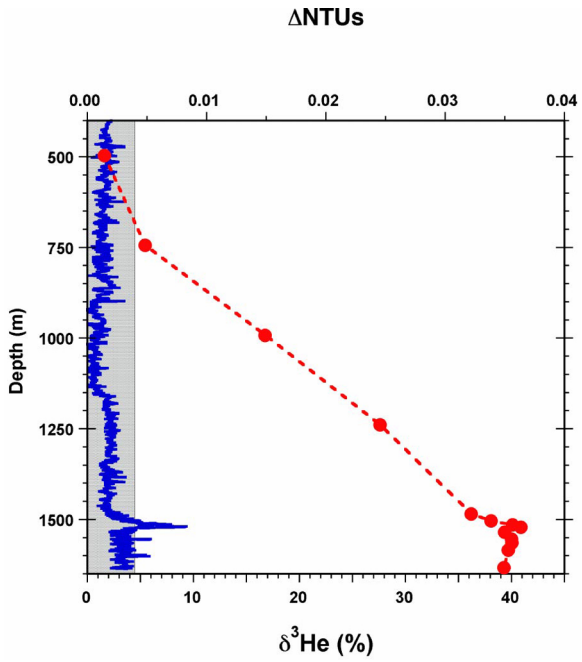

Figure 8. Expanded profile of δ^3He anomalies as measured in samples collected during the upcast at station CTD 24 on the FRSC (compare to Figure 7). Corresponding ΔNTU values for the CTD 24 upcast are also shown for comparison: gray shading indicates background optical backscatter values (ΔNTU < 0.004). Note that, unlike the case for TDFe and TDMn, δ^3He anomalies do not decrease to background values at depths immediately shallower than the top of the optically defined nonbuoyant plume.

δ^3He at ~1634 m. Consequently, the maximum δ^3He plume anomaly that can be attributed to the locally sourced plume at this station is no more than ~3%

3.3. Potential Sources for the Regional-Scale SW Pacific Hydrothermal Plume

[20] A prime motivation for this study was to investigate possible sources of a regional-scale hydrothermal plume, identified from mid-water ^{3}He anomalies, that appears to originate in the vicinity of the NE Lau Basin and propagate NW for at least 2000 km [*Lupton et al.*, 2004]. Although that plume was reported to exhibit a maximum plume anomaly at 1726 m at 15.0°S, 173.1°W (Figure 2), only 4 water samples were collected from that station between 1000 m and 2000 m water depth. Thus a more cautious approach would be to consider that the maximum plume anomaly for the SW Pacific regional-scale plume was constrained to lie between ~1500 m and 2000 m water depth. For comparison, at the next station west (14°54′S,179°00′W), *Lupton et al.* [2004] report results from 8 samples collected within the same depth range which reveal maximum δ^3He anomalies that are almost as large (41.2%) but are more tightly constrained, vertically, to lie close to 1500 m water depth. In combination, these two data sets could certainly be compatible with a single plume centered shallower than 2000 m, perhaps close to 1500 m water depth, which exhibits δ^3He anomalies significantly greater than 43% close to the NE corner of the Lau Basin.

[21] As shown in Figure 9, the plumes we have detected along the FRSC and NELSC are in partial fulfillment, at least, of these criteria. Both the southern FRSC plume (RC129) and the plumes further north on the FRSC at RC132 and DR59 lie within the predicted depth-range for the source of the regional-scale SW Pacific plume (1500–2000 m). However, at 17°01.5′S the only ^{3}He profile we have collected (CTD 24) indicates a maximum anomaly of δ^3He = 40.9% (Figures 7 and 8) which is lower than the maximum reported by *Lupton et al.* [2004] approximately 250 km distant (δ^3He = 43.4%). It seems unlikely therefore that this plume can be a significant source for the regional-scale SW Pacific Plume. For the other FRSC plumes, detected close to 16°45′S (RC 132) and 16°30′S (DR 59), maximum plume anomalies are deeper than at RC 129 (i.e., closer to the depth of the maximum δ^3He sample reported by *Lupton et al* [2004]), but the sizes of the ΔNTUs at these stations are also weaker than at RC129. We conclude therefore that these sites, too, cannot be considered as candidate point-sources for the SW Pacific regional-scale plume.

[22] The plume station near 15°23′S on the NELSC (RC 143, Figure 9) exhibits a much stronger ΔNTU than any plumes on the FRSC or, indeed, anywhere else along the NELSC. Although this plume is shallower than the 1500–2000 m depth range identified by *Lupton et al.* [2004], hydrothermal plumes can shoal by ~200 m when flowing over complex ridge topography [e.g., *German*, 2003] and this plume is located within 100–150 km of the stronger of the two δ^3He anomaly stations reported by *Lupton et al.* [2004]. Were ^{3}He-anomalies to scale linearly with ΔNTU in this NELSC plume, however, with a ratio identical to that for the plume sampled by CTD 24, we would only predict a maximum δ^3He of ~50% at this site on the NELSC. Although this signal is stronger

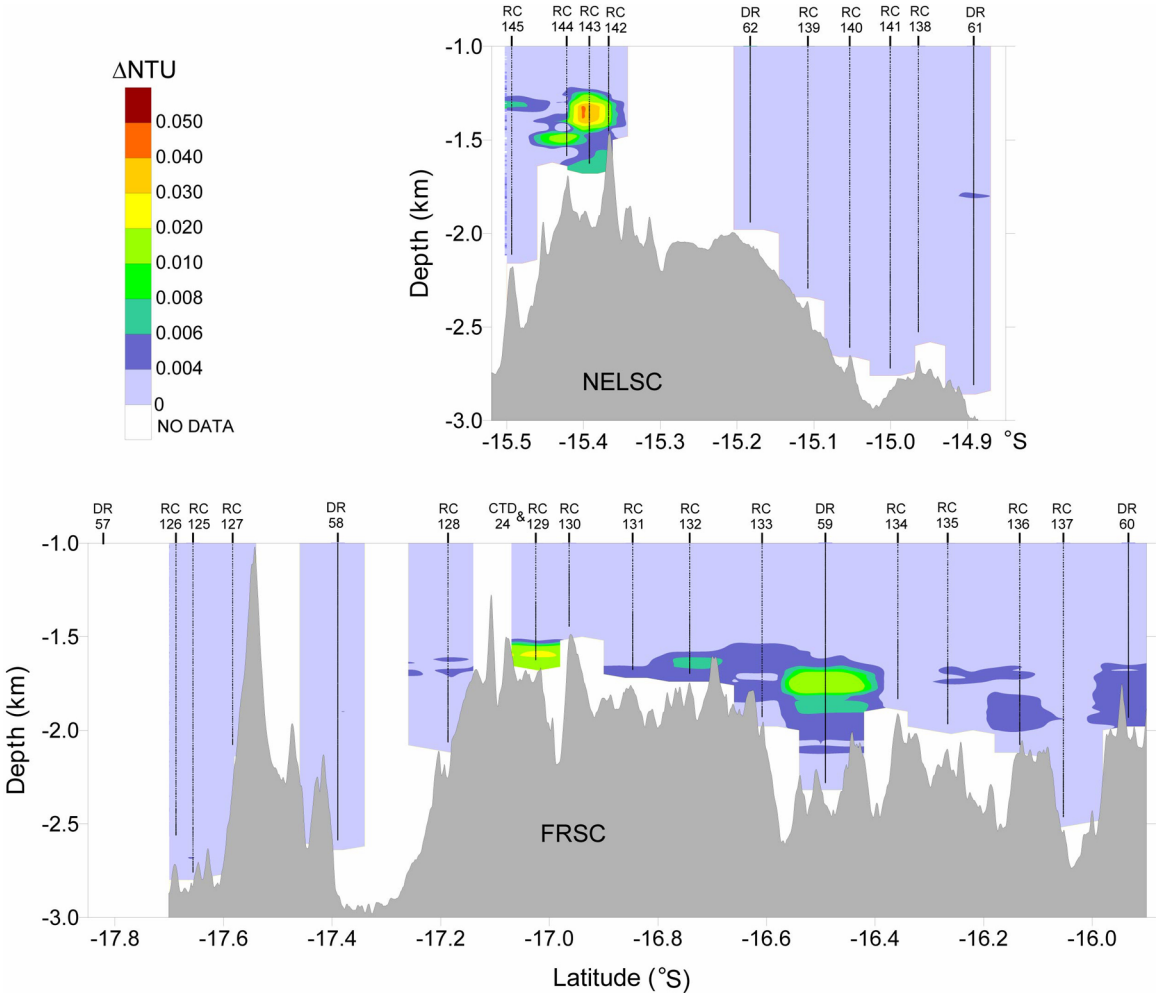

Figure 9. Cross sections of along-axis contoured optical backscatter anomalies (ΔNTU) overlying the "center-line" bathymetry of the neovolcanic ridge axis of (top) the Northeast Lau Spreading Center (NELSC) and (bottom) the Fonualei Rift and Spreading Center (FRSC). Vertical black lines show locations of individual MAPR profiles from which the contoured ΔNTU cross sections are derived. Lowest contour interval (0.004) is 3 sigma above the local ambient NTU value. Each profile was lowered to <50 m above the local bottom, although complex rough bathymetry can make the deepest data acquisition appear shallow with respect to the projected bathymetry along the ridge axis. Station locations, along with the water depths actually encountered at each sampling station, are listed in Table 1.

than the highest δ^3He values reported by *Lupton et al.* [2004], however, we do not consider any of the signals that we have detected to be sufficient to represent a viable point-source for the SW Pacific regional-scale plume, anywhere along the NELSC or FRSC in the NE Lau Basin. Instead, we consider that a more reasonable explanation for the source of the regional-scale SW Pacific plume is that it results from the cumulative discharge from numerous hydrothermal systems along the length of the Lau back-arc system, including those segments investigated here, being discharged into the open Pacific from the NE corner of this topographically restricted basin. Insight into the feasibility of such a process can be drawn from an on-going study of Lau Basin circulation (A. Thurnherr and K. Speer, PIs) conducted using autonomous floats that have been programmed to drift at a depth of ~1730 m, directly comparable to the depths of both hydrothermal plumes identified in this study and that of the SW Pacific regional-scale plume. While the first floats released, along the length of ELSC and VFR in Spring 2004, remain "trapped" within the south and central Lau Basin, two further floats, deployed in the westernmost Lau Basin during our cruise (KM 0417, September 2004), migrated to the NE corner of the Lau Basin in Spring 2005. One of these floats subsequently passed from ~16°30′S to north of 15°00′S along longitude ~175°S, effectively passing directly along the

FRSC and southernmost NELSC at plume-height, during the first 3 months of 2006 before being advected due west at 15°S as far as 176°W by late June; the other float remains "trapped" within the NE Lau Basin. (See latest updates at http://www.ldeo.columbia.edu/~ant/LAUB-FLEX/.)

4. Conclusions

[23] 1. We have identified hydrothermal plume signals in four areas, indicative of three discrete sources of high-temperature seafloor venting along the Fonualei Rift and Spreading Center (FRSC) and one further site on the Northeast Lau Spreading Center (NELSC) in the NE Lau Basin, regions previously unexplored for hydrothermal activity.

[24] 2. Maximum TDFe and TDMn concentrations in plume-samples collected from above the southernmost site reach concentrations of 18.8 nmol/kg and 13.4 nmol/kg. Dissolved ^{3}He anomalies in these samples reach a maximum of δ^3He ~41% representing a local enrichment of no more than ~3% superimposed on a larger basin-wide enrichment, observed throughout the deep-water column, that increases from δ^3He values of 5.5% at ~750 m to almost 40% below 1600 m.

[25] 3. While we have found no evidence for a single, large hydrothermal point-source in the NE Lau Basin, evidence now exists for numerous hydrothermal fields along the entire length of this multi-segment, fast-spreading, complex back-arc system. Therefore we conclude that the regional-scale ^{3}He-rich plume observed, extending up to 2000 km across the SW Pacific Ocean, most probably results from the cumulative hydrothermal output of the topographically restricted but hydrothermally active Lau Basin, discharging from its NE-most corner.

Acknowledgments

[26] We thank the Captain, officers, and crew of the R/V *Kilo Moana* during cruise KM0417 to the Lau Basin, September–October 2004. This research was funded jointly by NSF's Ridge 2000 Program (OCE-0242002 and OCE-0242618), by the NOAA Vents Program, and by core strategic funding from the Natural Environment Research Council to the National Oceanography Centre, Southampton (UK). PMEL contribution 2920.

References

American Public Health Association (1985), *Standard Methods for the Examination of Water and Wastewater*, 16th ed., 1268 pp., Washington, D. C.

Baker, E. T., and C. R. German (2004), On the global distribution of mid-ocean ridge hydrothermal vent-fields, in *The Thermal Structure of the Oceanic Crust and the Dynamics of Seafloor Hydrothermal Circulation*, *Geophys. Monogr. Ser.*, vol. 148, edited by C. R. German, J. Lin, and L. M. Parson, pp. 245–266, AGU, Washington, D. C.

Baker, E. T., M. Cormier, C. H. Langmuir, and K. Zavala (2001a), Hydrothermal plumes along segments of contrasting magmatic influence, 15°20′–18°30′N, East Pacific Rise: Influence of axial faulting, *Geochem. Geophys. Geosyst.*, *2*(9), doi:10.1029/2000GC000165.

Baker, E. T., D. A. Tennant, R. A. Feely, G. T. Lebon, and S. L. Walker (2001b), Field and laboratory studies on the effect of particle size and composition on optical backscattering measurements in hydrothermal plumes, *Deep Sea Res., Part I*, *48*, 593–604.

Baker, E. T., G. J. Massoth, K. Nakamura, R. W. Embley, C. E. J. de Ronde, and R. J. Arculus (2005), Hydrothermal activity on near-arc sections of back-arc ridges: Results from the Mariana Trough and Lau Basin, *Geochem. Geophys. Geosyst.*, *6*, Q09001, doi:10.1029/2005GC000948.

Baker, E. T., J. A. Resing, S. L. Walker, F. Martinez, B. Taylor, and K. Nakamura (2006), Abundant hydrothermal venting along melt-rich and melt-free ridge segments in the Lau back-arc basin, *Geophys. Res. Lett.*, *33*, L07308, doi:10.1029/2005GL025283.

Bird, P. (2003), An updated digital model of plate boundaries, *Geochem. Geophys. Geosyst.*, *4*(3), 1027, doi:10.1029/2001GC000252.

Corliss, J. B., M. Lyle, and J. Dymond (1978), The chemistry of hydrothermal mounds near the Galapagos rift, *Earth Planet Sci. Lett.*, *40*, 12–24.

Desbruyeres, D., et al. (1994), Deep-sea hydrothermal communities in Southwestern Pacific back-arc basins (the North-Fiji and Lau Basins): Composition, micro-distribution and food-web, *Mar. Geol.*, *116*, 227–242.

Edmonds, H. N., P. J. Michael, E. T. Baker, D. P. Connelly, J. E. Snow, C. H. Langmuir, H. J. B. Dick, R. Mühe, C. R. German, and D. W. Graham (2003), Discovery of abundant hydrothermal venting on the ultraslow-spreading Gakkel Ridge, Arctic Ocean, *Nature*, *421*, 252–256.

Edmonds, H. N., C. R. German, J. A. Breier, D. P. Connelly, A. Townsend-Small, J. A. Resing, C. Aumack, E. T. Baker, and C. H. Langmuir (2004), Plume mapping and shipboard geochemical data used to locate new vent sites in the Lau Basin, *Eos Trans. AGU*, *85*(47), Fall Meet. Suppl., Abstract B13A-0191.

Feely, R. A., G. J. Massoth, and G. T. Lebon (1991), Sampling of marine particulate matter and analysis by x-ray fluorescence spectrometry, in *Marine Particles: Analysis and Characterization*, *Geophys. Monogr. Ser.*, vol. 63, edited by D. C. Hurd and D. W. Spencer, pp. 251–257, Washington, D. C.

Field, M. P., and R. M. Sherrell (2000), Dissolved and particulate Fe in a hydrothermal plume at 9 degrees 45′N, East Pacific Rise: Slow Fe (II) oxidation kinetics in Pacific plumes, *Geochim. Cosmochim. Acta*, *64*, 619–628.

Fouquet, Y., et al. (1991), Hydrothermal activity in the Lau back-arc basin: Sulfides and water chemistry, *Geology*, *19*, 303–306.

German, C. R. (2003), Hydrothermal activity on the eastern SWIR (50°–70°E): Evidence from core-top geochemistry, 1887 and 1998, *Geochem. Geophys. Geosyst.*, *4*(7), 9103, doi:10.1029/2003GC000522.

German, C. R., and K. L. Von Damm (2004), Hydrothermal Processes, in *Treatise on Geochemistry*, vol. 6, edited by H. D. Holland and K. K. Turekian, pp. 181–222, Elsevier, New York.

German, C. R., E. T. Baker, C. A. Mevel, K. Tamaki, and the FUJI Scientific Team (1998), Hydrothermal activity along the South West Indian Ridge, *Nature*, *395*, 490–493.

German, C. R., R. A. Livermore, E. T. Baker, N. I. Bruguier, D. P. Connelly, A. P. Cunningham, P. Morris, I. P. Rouse, P. J. Statham, and P. A. Tyler (2000), Hydrothermal plumes above the East Scotia Ridge: An isolated high-latitude back-arc spreading centre, *Earth Planet. Sci. Lett.*, *184*, 241–250.

German, C. R., D. P. Connelly, R. D. Prien, D. Yoerger, M. Jakuba, A. Bradley, T. J. Shank, H. N. Edmonds, and C. H. Langmuir (2004), New techniques for hydrothermal exploration: In situ chemical sensors on AUVs—Preliminary results from the Lau Basin, *Eos Trans. AGU*, *85*(47), Abstract B13A-0190.

Hart, S. R., et al. (2000), Vailulu'u undersea volcano: The New Samoa, *Geochem. Geophys. Geosyst.*, *1*(12), doi:10.1029/2000GC000108.

Ishibashi, J., J. E. Lupton, T. Yamaguchi, J. Querellou, T. Nunoura, and K. Takai (2006), Expedition reveals changes in Lau Basin hydrothermal system, *Eos Trans. AGU*, *87*, 13–16.

Langmuir, C. H., et al. (2005), Vent discovery and petrological sampling of the Lau Back Arc Basin, *R/V Kilo Moana KM 0417 Cruise Rep.*, 82 pp., Natl. Sci. Found., Washington, D. C.

Livermore, R. (2003), Back-arc spreading and mantle flow in the East Scotia Sea, in *Intra-oceanic Subduction Systems: Tectonic and Magmatic Processes*, edited by R. D. Larter and P. T. Leat, *Geol. Soc. Spec. Publ.*, *219*, 315–331.

Lupton, J. E. (1990), Water column hydrothermal plumes on the Juan de Fuca Ridge, *J. Geophys. Res.*, *95*, 12,829–12,842.

Lupton, J. E., and H. Craig (1981), A major ^{3}He source on the East Pacific Rise, *Science*, *214*, 13–18.

Lupton, J. E., D. G. Pyle, W. J. Jenkins, R. Greene, and L. Evans (2004), Evidence for an extensive hydrothermal plume in the Tonga-Fiji region of the South Pacific, *Geochem. Geophys. Geosyst.*, *5*, Q01003, doi:10.1029/2003GC000607.

Magnusson, B., and S. Westerlund (1981), Solvent extraction procedures combined with back-extraction for trace metal determination by atomic absorption spectrometry, *Anal. Chim. Acta*, *131*, 63–72.

Martinez, F., and B. Taylor (2003), Controls on back-arc crustal accretion: Insights from the Lau, Manus, and Mariana basins, in *Intra-oceanic Subduction Systems: Tectonic and Magmatic Processes*, edited by R. D. Larter and P. T. Leat, *Geol. Soc. Spec. Publ.*, *219*, 19–54.

Martinez, F., B. Taylor, E. T. Baker, J. A. Resing, and S. L. Walker (2006), Opposing trends in crustal thickness and spreading rate along the back-arc Eastern Lau Spreading Centre: Implications for controls on ridge morphology, faulting and hydrothermal activity, *Earth Planet. Sci. Lett.*, *245*, 655–672.

Pelletier, B., Y. Lagabrielle, M. Benoit, G. Cabioch, S. Calmant, E. Garel, and C. Guivel (2001), Newly identified segments of the Pacific-Australia plate boundary along the North Fiji transform zone, *Earth Planet. Sci. Lett.*, *193*, 347–358.

Rudnicki, M. D., and C. R. German (2002), Temporal variability of the hydrothermal plume above the Kairei vent field, 25°S, Central Indian Ridge, *Geochem. Geophys. Geosyst.*, *3*(2), 1010, doi:10.1029/2001GC000240.

Rudnicki, M. D., R. H. James, and H. Elderfield (1994), Near-field variability of the TAG non-buoyant plume, 26°N, Mid-Atlantic Ridge, *Earth Planet. Sci. Lett.*, *127*, 1–10.

Scheirer, D. S., E. T. Baker, and K. M. Johnson (1998), Detection of hydrothermal plumes along the Southeast Indian Ridge near the Amsterdam-St. Paul hotspot, *Geophys. Res. Lett.*, *25*, 97–100.

Statham, P. J., C. R. German, and D. P. Connelly (2005), Iron (II) distribution and oxidation kinetics in hydrothermal plumes at the Kairei and Edmond vent sites, Indian Ocean, *Earth Planet. Sci. Lett.*, *236*, 588–596.

Staudigel, H., et al. (2006), Vailulu'u Seamount, Samoa: Life and death on an active submarine volcano, *Proc. Natl. Acad. Sci. U. S. A.*, *103*, 6448–6453.

Turner, S., and C. Hawkesworth (1998), Using geochemistry to map mantle flow beneath the Lau Basin, *Geology*, *26*, 1019–1022.

Tyler, P. A., C. R. German, E. Ramirez-Llodra, and C. L. Van Dover (2002), ChEss: Understanding the biogeography of chemsynthetic ecosystems*Oceanol. Acta*, *25*, 227–241.

Van Dover, C. L., et al. (2001), Biogeography and ecological setting of Indian Ocean hydrothermal vents, *Science*, *294*, 818–823.

Van Dover, C. L., C. R. German, K. G. Speer, L. M. Parson, and R. C. Vrijenhoek (2002), Evolution and biogeography of deep-sea vent and seep invertebrates, *Science*, *295*, 1253–1257.

Walker, S. L., E. T. Baker, G. J. Massoth, and R. N. Hey (2004), Short-term variations in the distribution of hydrothermal plumes along a superfast spreading center, East Pacific Rise, 27°30′–32°20′S, *Geochem. Geophys. Geosyst.*, *5*, Q12005, doi:10.1029/2004GC000789.

Young, C. E., and J. E. Lupton (1983), An ultra-tight fluid sampling system using cold-welded copper tubing, *Eos Trans. AGU*, *64*, 735.

Zellmer, K. E., and B. Taylor (2001), A three-plate kinematic model for Lau Basin opening, *Geochem. Geophys. Geosyst.*, *2*(5), doi:10.1029/2000GC000106.